Journal of Colloid and Interface Science 582 (2021) 51–59

Contents lists available at ScienceDirect

Journal of Colloid and Interface Science

journal homepage: www.elsevier.com/locate/jcis

Impact of carbonate-based electrolytes on the electrochemical activity of carbon-coated $Na_3V_2(PO_4)_2F_3$ cathode in full-cell assembly with hard carbon anode

Krishnan Subramanyan [a], Yun-Sung Lee [b], Vanchiappan Aravindan [a,*]

[a] Department of Chemistry, Indian Institute of Science Education and Research (IISER), Tirupati 517507, India
[b] Department of Advanced Chemicals and Engineering, Chonnam National University, Gwang-ju 61186, Republic of Korea

GRAPHICAL ABSTRACT

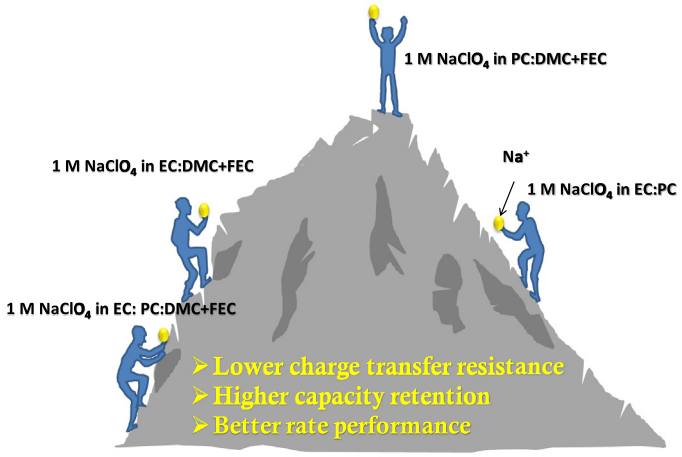

ARTICLE INFO

Article history:
Received 1 July 2020
Revised 10 August 2020
Accepted 11 August 2020
Available online 11 August 2020

Keywords:
Sodium-ion batteries
$Na_3V_2(PO_4)_2F_3$
Hard carbon
Electrolytes
In-situ impedance

ABSTRACT

An immense effort has been put into developing high-performance electrodes to commercialize sodium-ion batteries, but research on developing an efficient electrolyte is lacking. This study aims to find the best carbonate-based electrolyte systems by incorporating the existing ideas reported in this field. The sodium superionic conductor (NASICON) type $Na_3V_2(PO_4)_2F_3$-C (NVPF-C) was chosen as a cathode, and its compatibility with four different carbonate-based electrolyte solutions was studied in the half-cell assembly. Additionally, full-cell assembly with hard carbon as an anode is also explored. Binary and ternary combinations of the solvents ethylene carbonate, propylene carbonate, and dimethyl carbonate were employed with and without fluoroethylene carbonate as an additive. A systematic study was performed, including the *in-situ* impedance technique, and to determine the compatibility. Detailed galvanostatic studies for NVPF-C based half-cells, as well as hard carbon/NVPF-C full-cells, are performed, which shows that 1 M $NaClO_4$ in propylene carbonate:dimethyl carbonate + fluoroethylene carbonate is a better electrolyte composition for this assembly. Subsequently, a temperature study was carried out on this electrolyte to test its performance.

* Corresponding author.
E-mail address: aravind_van@yahoo.com (V. Aravindan).

https://doi.org/10.1016/j.jcis.2020.08.043
0021-9797/

1. Introduction

The diminishing fossil fuel resources drive the energy production sector to promote renewable energy resources, whose intermittent nature requires the employment of energy storage devices. Batteries have been the preferred choice of energy storage devices [1]. Particularly, lithium-ion batteries (LIB) are regarded as the holy grail of energy storage devices because of their high energy density, long cycling stability, and light-weight build [2]. It has been gaining more importance with recent efforts in efficiently recycling the spent batteries [3,4]. Due to the limited resources and uneven geographical distribution, an impending lithium shortage and fluctuations in the supply chain are predicted. Statistics show that the battery industry consumes a significant share of the extracted lithium, and unless the recycling process is increased manifold, the LIB industry will be acutely affected [5]. In addition to this, LIB poses a large number of safety issues, such as lithium plating and thermal runaway. The increasing prices of the transition metals used in LIBs (cobalt, nickel, chromium, etc.) and copper current collector drives up the cost per kWh of LIB [6–8]. Due to the reduced production cost and improved safety, sodium-ion batteries (SIB) have regained their attention as a possible alternative to the existing LIB [9,10]. Even though many works have been done on developing high energy, stable electrode systems, very few reports on electrolytes are currently available. By employing an appropriate electrolyte, a significant improvement in battery performance is possible.

An obstacle in developing high-performance SIB is the unavailability of a universal electrolyte, unlike the LIB systems. The stability of the electrolyte and the passivation layers formed are vital to the performance of a cell. During charge and discharge, the electrolyte in the cell is exposed to cathode and anode surfaces. It is also subjected to large voltage variations during charge–discharge of the cell. Owing to the electrolyte dissociation, a passivation layer, commonly known as a solid electrolyte interface (SEI), is formed on the electrode surface. The SEI should be highly conducting, but it should be stable during the charge–discharge cycles. This SEI layer is critical for the cells' long-term cycling stability since a poor SEI layer can lead to continuous electrolyte decomposition leading to a gradual decay of the cell capacity. It was also found that the SEI layer formed in SIBs is less sturdy when compared to LIBs, which suggests that more effort has to be put into the electrolyte development for SIBs [11]. The carbonate-based electrolyte systems have been used as a standard electrolyte for LIB, and profound progress has been made to optimize the same for SIB. Ponrouch *et al.* [12] conducted a study to optimize the carbonate-based sodium-ion battery electrolyte by employing a tertiary electrolyte system. The optimization of the electrolyte system was carried out by varying the third component, and its volume. Before this, they also conducted a study on various carbonate-based electrolytes to obtain the best combination possible for the hard-carbon system [13]. Bhide *et al.* [14] performed a conductivity study to determine the optimum concentration of electrolyte salts in a binary mixture of carbonate solvents. A study on the influence of ionic liquids added to carbonate-based electrolytes and volume to be added to maximize the performance was conducted by Monti *et al.* [15]. Vidal-Abarca *et al.* [16] proved that the choice of electrolyte heavily influenced the performance and the cycling stability of the cell. Myriad review articles are available, which compare the electrolytes in the reported literature to provide a comprehensive idea on various types of electrolyte systems and their pros and cons [11,17–20].

This work attempts to obtain the optimum carbonate-based electrolyte system for a sodium-ion cell with hard carbon as anode and $Na_3V_2(PO_4)_2F_3$-C (NVPF-C) as a cathode with focus on the electrochemical performance of the sodium half/full-cell. Besides carbon coating, the novel material such as graphdiyne coating may also be tried [21–23]. NVPF-C has two redox peaks at ~3.5 V and ~4.0 V (*vs.* Na/Na^+), providing us an opportunity to study the formation of interface films due to electrolyte decomposition *via* impedance study. A major share of carbonate-based electrolytes uses the salts $NaClO_4$ or $NaPF_6$, whereas NaFSI, NaTFSI, etc. are meagerly used [11]. Ponrouch *et al.* [13] had demonstrated that the electrolyte salts $NaClO_4$ and $NaPF_6$ exhibited similar performances. Hence the salt used throughout this study was $NaClO_4$ at 1 M concentration in various carbonate-based binary and ternary solvents. Rather than using a single-solvent base electrolyte system, we test the half/full-cell performance with binary and ternary electrolytes, which have improved ionic conductivity, lower viscosity, and stability over a wide potential window [11,12]. The electrolytes used in this study were propylene carbonate:dimethyl carbonate + fluoroethylene carbonate (PC:DMC + FEC, 1:1 vol + 5 vol%), ethylene carbonate:dimethyl carbonate + fluoroethylene carbonate (EC:DMC + FEC, 1:1 vol + 5 vol%), ethylene carbonate:propylene carbonate (EC:PC, 1:1 vol), and ethylene carbonate:propylene carbonate:dimethyl carbonate + fluoroethylene carbonate (EC:PC:DMC + FEC, 0.45:0.45:0.1 vol + 5 vol%). PC and EC have been elaborately used for the Li-ion batteries owing to its high dielectric constant, which bolsters the sodium salt dissociation. The co-solvent DMC was chosen to reduce the electrolyte's viscosity, thereby promoting the ion transfer rates. Moreover, the EC:DMC has been found to form a eutectic mixture, providing a better performance at room temperature. Fluoroethylene carbonate has been chosen as an additive since it supports better and robust SEI formation. For hard carbon anode, the EC:PC is the most suitable electrolyte solvent, and this electrolyte has been adopted without the additive [24]. This provides an opportunity to validate whether the improved performance of hard-carbon alone enhances the full-cell performance.

2. Experimental section

2.1. Synthesis

NVPF-C was synthesized through a reported procedure [25]. In a typical synthesis process, 50 mL distilled water, stoichiometric amounts of Na_2CO_3 (Sigma Aldrich, >99%), $NH_4H_2PO_4$ (Sigma Aldrich, >98%), NaF (Sigma Aldrich, >99%), and V_2O_5 (Sigma Aldrich, >98%) was dissolved and thoroughly dried in a forced-air oven at 50 °C. To the above precursor, acetylene black (5 wt% of the total mass of the reagents) was added and grounded well. The above mixture was subjected to 350 °C for 4 h under argon flow with a ramp rate of 5 °C $min.^{-1}$, which was then reground well followed by another heating at 650 °C for 8 h under argon flow with a ramp rate of 5 °C $min.^{-1}$. The above-obtained material was ground to a fine powder using a mortar and pestle to get NVPF-C. Hard carbon was gratis provided by Kuraray (Kuranode, type 3, Japan) and was directly used as the active material for the anode.

2.2. Electrolyte preparation

The electrolytes were prepared inside the glove box with $NaClO_4$ salt (Sigma Aldrich, 98%) dissolved in various solvents such as propylene carbonate (PC, Sigma, anhydrous, 99.7%), ethylene carbonate (EC, Sigma, anhydrous, 99%), dimethyl carbonate (DMC, Sigma, anhydrous, >99%), and additive fluoroethylene carbonate (FEC, Sigma, anhydrous, >99%) in binary and ternary combi-

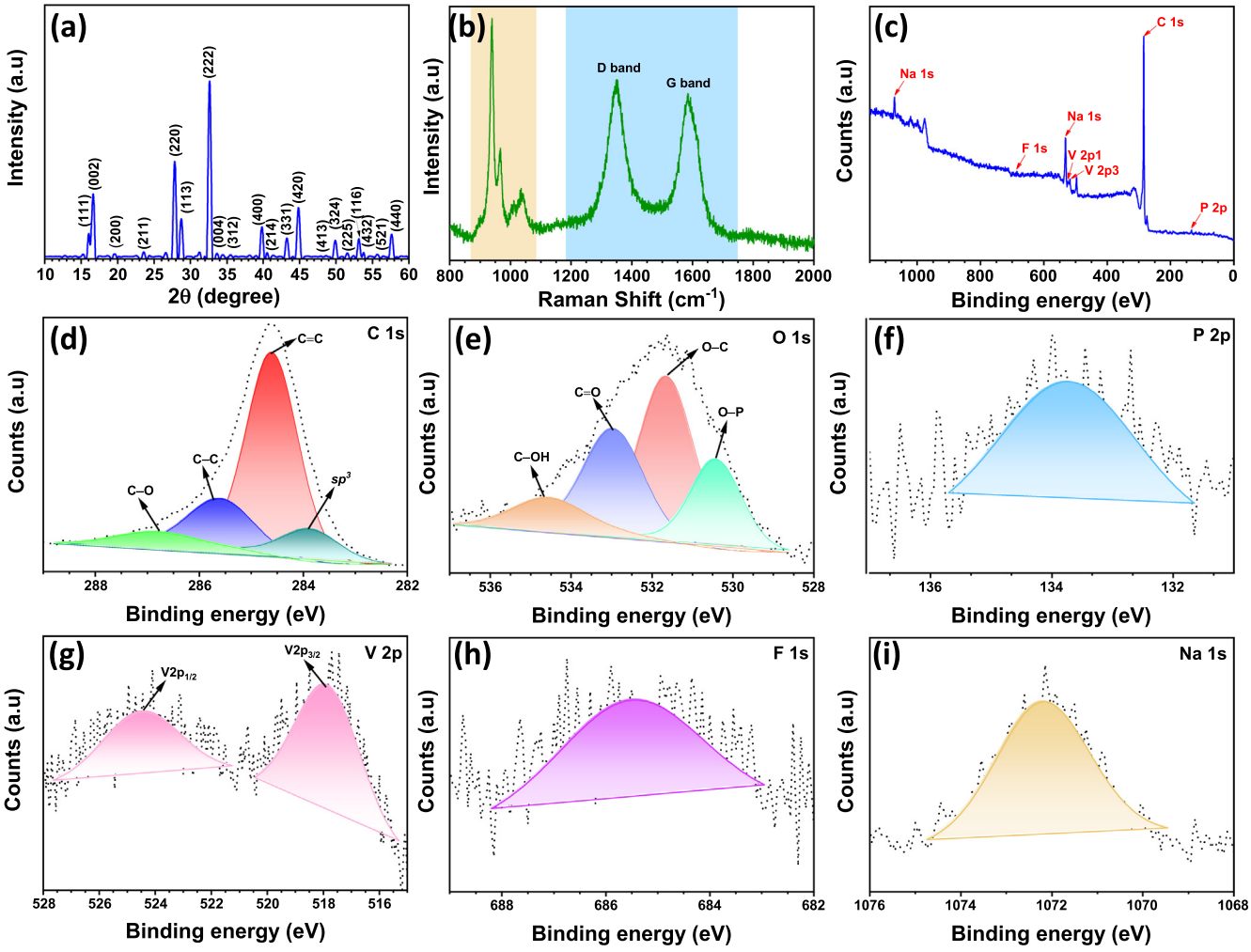

Fig. 1. (a) XRD pattern for the synthesized NVPF-C, (b) Raman spectra of the NVPF-C showing the peak corresponding to PO_4 group (highlighted in brown), D band, and G band (highlighted in blue), (c) XPS spectra for the as-synthesized NVPF-C showing the elements present, and (d-i) high-resolution spectra of O1s, P2p, V2p, F1s and Na1s.

nations. The salts, and the solvents, were directly used without any form of purification or pre-treatment.

2.3. Material characterization

The structural characterization of NVPF-C was carried out through X-ray diffraction (XRD, ULTIMA-IV, Rigaku, ARBL-RAD), and material composition was determined through Raman spectroscopy (LabRam HR800 UV Raman microscope, Horiba Jobin-Yvon, France). The XRD analysis was done at a scanning rate of 1° min^{-1} with monochromatic Cu Kα radiation (λ = 1.5406 Å). Using a 515 nm diode laser as light source Raman spectra of the material was recorded at room temperature. The material's surface constituents were ensured through X-ray photoelectron spectroscopy (XPS, Multilab 2000, UK). Field emission scanning electron microscopy (FE-SEM S-4700, Hitachi, Japan) and high-resolution transmission electron microscopy (HR-TEM, JEM-2000, EX-II, JEOL, Japan) were employed for surface and internal structure, respectively.

2.4. Electrochemical characterization

All the half-cells and full-cells were fabricated in an argon-filled glove box (MBraun, Germany) with the oxygen and moisture level at < 0.1 ppm. Hard carbon (HC), conductive additive (acetylene black), and binder (polyvinylidene fluoride - PVdF) were mixed at a ratio of 75:10:15 (wt.%) in *N*-Methyl-2-pyrrolidone (NMP) to form a slurry. This slurry was coated on copper foil using a doctor blade apparatus followed by complete drying at 75 °C overnight. These were then cut into 14 mm diameter electrodes, which were kept at 75 °C in a vacuum oven and used in CR2016 coin cells with glass microfiber separators (Whatman, cat no. 1825-047, UK) with metallic sodium as counter-electrode. The composite electrode composed of 10 mg of NVPF-C, 2 mg of conductive additive (acetylene black), and 2 mg binder (teflonized acetylene black-2, TAB), which were mixed in a mortar pestle with ethanol into a freestanding film. Later, the film was pressed onto a 16 mm diameter stainless steel mesh (Goodfellow, UK), which acted as the current collector. These were kept overnight at 75 °C in a vacuum oven to make the test cells with metallic sodium as counter-electrode for the half-cell assembly in CR2016 coin cells. Before the balanced full-cell fabrication, the hard-carbon half-cells were subjected to 3 cycles of charge–discharge, and the cell was de-crimped to remove the hard-carbon electrode carefully. The mass of active material in the NVPF-C electrode was adjusted according to the former one's capacity, and full-cells were fabricated with glass microfiber separator. The gravimetric capacities of full-cell were calculated based on active material loading in the anode, *i.e.,* hard carbon.

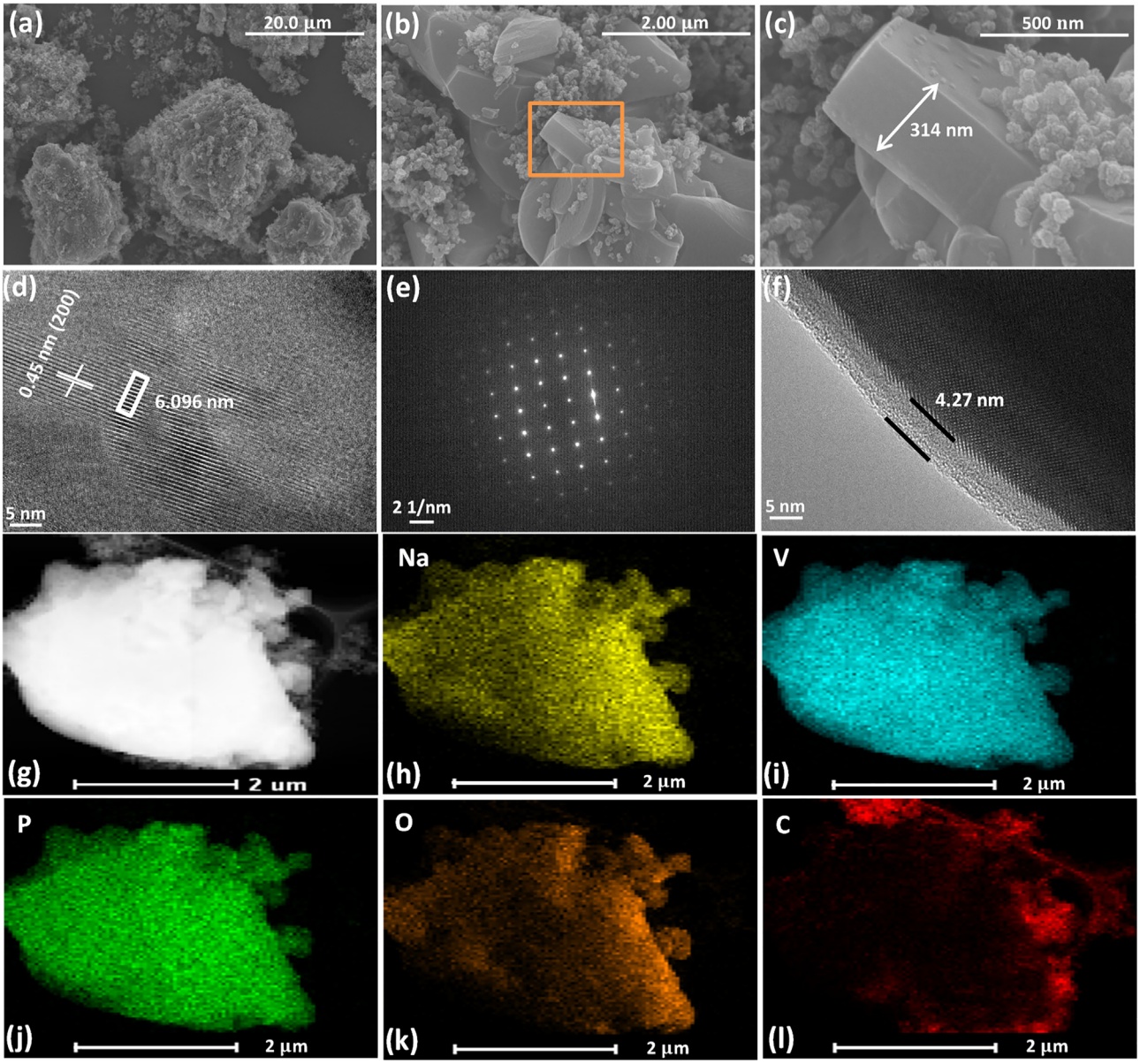

Fig. 2. (a-c) FE-SEM images of NVPF-C, (d and f) HR-TEM images of NVPF-C, (e) SAED pattern of NVPF-C, (g-l) EDS elemental mapping of NVPF-C showing the elemental distribution of Na, V, P, O and C.

3. Results and discussion

The structural features of the synthesized NVPF-C were analyzed through powder XRD. An XRD analysis of the as-synthesized NVPF-C (Fig. 1a) is consistent with the previous report, and the diffraction peaks suggest a tetragonal structure belonging to the $P4_2/mnm$ space group [25]. The refined unit cell parameters were calculated as $a = b = 9.07$ Å, $c = 10.658$ Å, and V = 876.78 Å^3 from the XRD pattern. The prominent reflections at the 2θ values of 16.12°, 16.62°, 27.82°, 28.74°, and 32.62° correspond to the crystal planes (111), (002), (220), (113), and (222), respectively. The structure of NVPF-C can be described as a 3D NASICON (sodium superionic conductor) type structure built up by a bi-octahedral structure [$V_2O_8F_3$] (a combination of two [VO_4F] connected *via* an F) and [PO_4] tetrahedral units. Better rate performance is probable by this structure *via* a higher rate of Na-ion diffusion distributed in the NASICON network in both X and Y directions [26]. The Raman spectra (Fig. 1b) of NVPF-C shows two peaks at 1350 cm^{-1} and 1584 cm^{-1} corresponding to the D band and the G band, which are indications of disordered carbon and graphitized carbon respectively. The degree of disorderness is calculated from these peaks from the I_D/I_G ratio, which is 1.051 in this case. This indicates that the carbon is mostly present in the amorphous state. The highlighted region in the Raman spectra displays two peaks centered at ~930 cm^{-1} and ~1040 cm^{-1}, which arise due to the symmetric and asymmetric stretching of the P—O bond in the PO_4 group[27]. For determining the elemental composition of the prepared compound, XPS analysis was carried out. The XPS survey spectrum (Fig. 1c) indicated the presence of Na, F, O, V, C, and P. The chemical state of these elements was evaluated by deconvoluting of C1s, O1s, P2p, V2p, F1s, and Na1s core levels (Fig. 1d-i). The C1s peak can be decomposed into four peaks at 283.9, 284.6, 285.6, and 286.9 eV, which corresponds to the sp^3 carbon, C═C, C—C, and C—O coordination, respectively [28,29]. The deconvolution of the

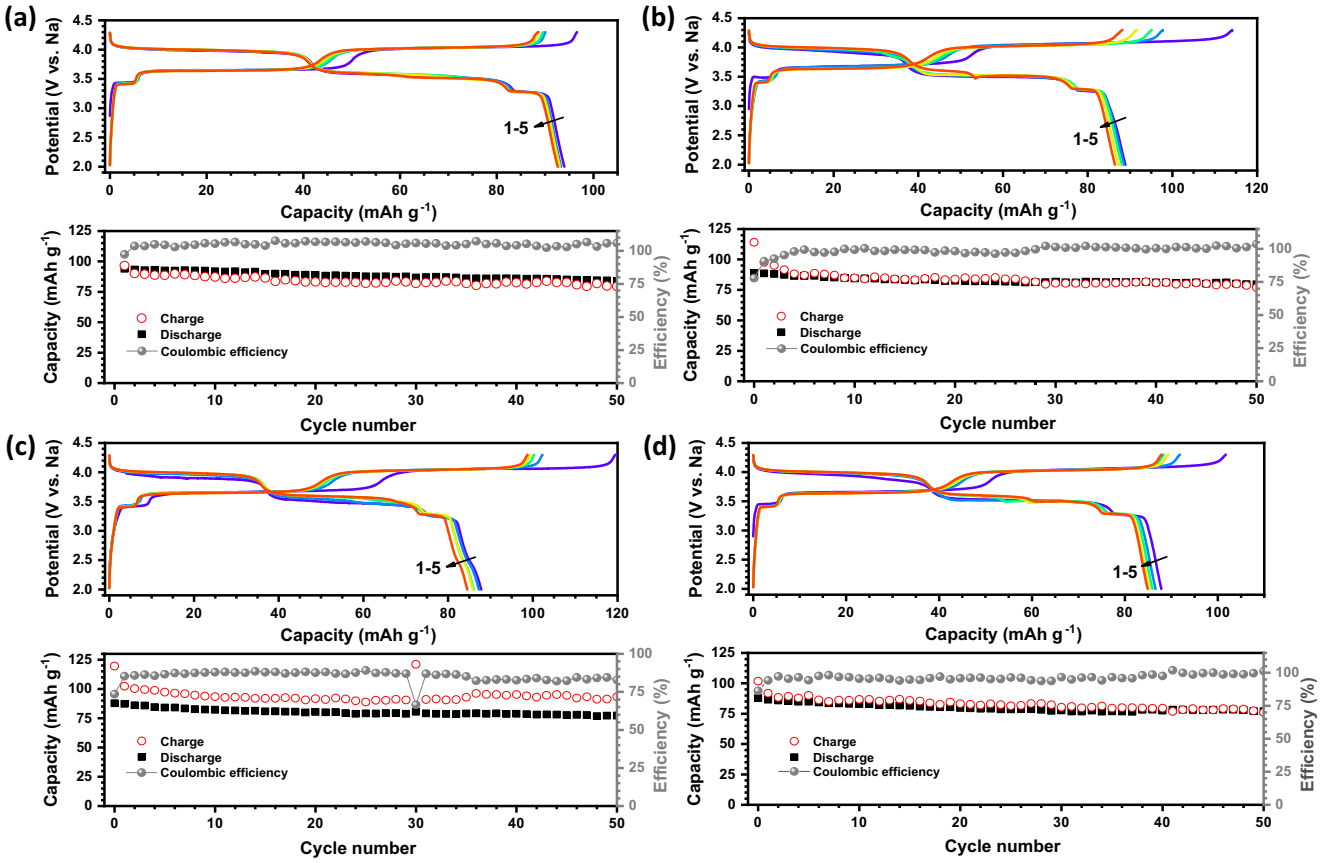

Fig 3. Charge-discharge curves for initial five cycles and the long-term cycling performance of NVPF-C in half-cell assembly with 1 M $NaClO_4$ in (a) PC:DMC + FEC, (b) EC:DMC + FEC, (c) EC:PC, and (d) EC:PC:DMC + FEC electrolytes at 20 mA g^{-1} from 2 to 4.3 V *vs.* Na.

O1s core level yields four peaks at 530.45, 531.65, 532.95, and 534.6 eV, which belongs to O—P, O—C, O═C, and C—OH, respectively [30,31]. The spectrum at V2p core level has two broad peaks at $V2p_{3/2}$ and $V2P_{1/2}$ at 517.75, and 524.48 eV, whereas at 133.73 eV, 685.49 eV, and 1072.19 eV exhibits broad spectra which are affiliated to the P2p, F1s, and the Na1s core levels.

The micrographs obtained through FE-SEM (Fig. 2a, b, and c) reveal the particle's non-uniform size distribution with slight particle agglomeration. These have a semi-uniform carbon coating on the surface. The SEM images reveal that these agglomerations comprise of NVPF-C crystals, with one of them identified to have around 314 nm in dimensions. The TEM images (Fig S1) confirms the above observation. A closer look through HR-TEM (Fig. 2d) discloses the regular crystal structure of the NVPF-C lattice with the lattice fringes, separated at a distance of 0.45 nm, which matches with the (200) plane observed in the NVPF-C XRD pattern. The selected area electron diffraction pattern (SAED) (Fig. 2e) also confirms the existence of the regular periodic crystal structure of the material. The continuous planes seen in the image establishes the exceptional crystalline nature of the material synthesized. A thin uniform layer of carbon (~4.27 nm) is visible on the NVPF-C surface (Fig. 2f), which helps to boost the otherwise poor electronic conductivity of the bare sodium vanadium fluorophosphate (10^{-7} S cm^{-1}) [27].

The energy dispersive X-ray spectrometry (EDS) images (Fig. 2-g-l) present the constituent elements' uniform distribution throughout the particle. The signals corresponding to sodium, vanadium, phosphorous, and oxygen are very homogenous and exactly coincide with the components of NVPF-C. This assures the consistent presence of NVPF-C. The carbon content is non-uniform, which may be due to the exposure of the carbon-coated copper grid.

3.1. Half-cell performance

The Fig. 3 shows the performance of NVPF-C in half-cell assembly for 1 M $NaClO_4$ in PC:DMC + FEC, EC:DMC + FEC, EC:PC, and EC:PC:DMC + FEC electrolytes. NVPF-C half-cell (NHC) with electrolytes PC:DMC + FEC, EC:DMC + FEC, EC:PC, and EC:PC:DMC + FEC are abbreviated as NHC-1, NHC-2, NHC-3, and NHC-4 respectively in the rest of the work. Other combinations of electrolytes with solvents even from the glyme family were tested, and their results are shown in Fig. S2. It can be seen that the irreversibility in the half-cell with EC as a co-solvent in the electrolyte is higher when compared to PC:DMC + FEC. This is caused due to the decomposition of EC at 4.3 V *vs.* Na. The decomposition of PC takes place at a higher voltage of > 4.5 V *vs.* Na, which is not observed here as the upper voltage is capped at 4.3 V *vs.* Na [32]. The other factor contributing to the irreversibility is the decomposition of DMC, which takes place around 3.30 and 3.94 V *vs.* Na [33]. The high permittivity of PC coupled with its ease of forming a protective layer with the least amount of additives/co-solvents makes it a perfect solvent choice [34]. The irreversible decomposition of FEC would contribute equally in all the electrolytes used, contributing to the initial irreversibility and, in turn, assisting the formation of a more robust SEI layer. The cycling profile at 20 mA g^{-1} reveals that after 50 cycles, NHC-1 exhibited maximum capacity retention of 82% (initial charge capacity: 97 mAh g^{-1}),

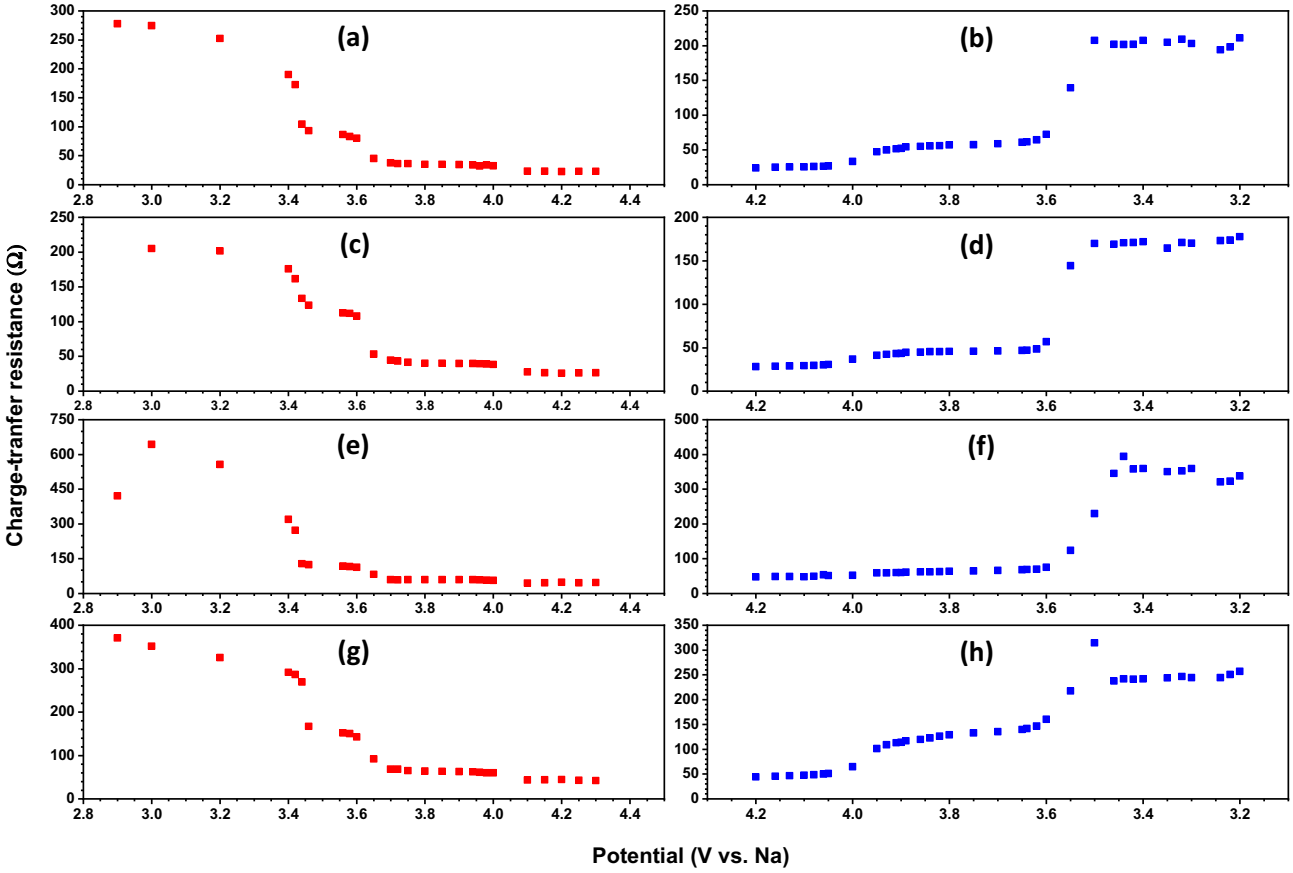

Fig. 4. Charge-transfer resistance for charging and discharging (red and blue respectively) for NVPF-C half-cell with 1 M $NaClO_4$ in (a, b) PC:DMC + FEC, (c,d) EC:DMC + FEC, (e, f) EC:PC, and (g,h) EC:PC:DMC + FEC electrolytes.

whereas NHC-2 exhibited the least capacity retention of 67% (initial charge capacity: 114 mAh g^{-1}). The NHC-3 (initial charge capacity: 120 mAh g^{-1}) and NHC-4 (initial charge capacity: 102 mAh g^{-1}) exhibited capacity retention of 78 and 75%, respectively. The NHC-3 exhibited the highest initial capacity of 120 mAh g^{-1} but failed to exhibit better CE (Coulombic efficiency) throughout the cycling process. This can be accounted for by the inefficient SEI layer formed on the electrode surface due to the absence of FEC additive. To further understand the electrochemical performance of such electrolytes, an *in-situ* impedance was performed in half-cell assembly.

An *in-situ* impedance study was performed to investigate the cause of the initial irreversibility and the improved performance of a particular electrolyte. The Nyquist plots of all the electrolytes at the voltage limits are shown in Fig. S3. The charge-transfer resistance for each case was calculated and plotted (Fig. 4). As hypothesized, one of the major causes of the irreversibility was the formation of a robust SEI layer, which is confirmed by the change in the charge transfer resistance (R_{CT}) after one complete charge–discharge. The charge-transfer resistance is least for the half-cell's fully charged state due to the minimum exchange current across the electrode and the electrolyte. The decomposition of the electrolyte constituent solvents leads to the formation of surface films. NHC-2 exhibited the least R_{CT} after cycling, whereas NHC-3 exhibited the highest R_{CT}. When the relative reduction in R_{CT} is considered$\left(\frac{initial\ \ R_{CT}-final\ \ R_{CT}}{initial R_{CT}} * 100\right)$, NHC-4 shows the maximum value (31%), whereas the least is NHC-2 (13%). NHC-1 shows a reasonable reduction of 23%, followed by NHC-3 at 20%. If the relative reduction of R_{CT} is considered, the SEI layer formed in NHC-4 displayed the most improvement in conductivity. This reduction of impedance matters because it shows the most effective layer formation on the cathode throughout the electrolytes tested, and NHC-1 shows excellent performance in both of the tests mentioned above. Hence, as far as the NVPF-C half-cell is considered, the best choice amongst the tested electrolytes is the electrolyte with PC:DMC + FEC as the solvent. Further, insight into the nature of the SEI formed with various electrolyte solutions is underway

3.2. Full-cell performance

The mass of cathode material was adjusted for the capacity of the hard carbon anode which was performed for the all the four electrolytes according to the equation

$$\boldsymbol{m_1 c_1 = m_2 c_2}$$

where m_1 and m_2 are the masses of the anode and cathode active material, and c_1 and c_2 are the capacities in mAh g^{-1} (wrt mass of the active material alone). Similarly, hard carbon electrode's irreversibility was mitigated by three charge–discharge cycles followed by assembly of the full-cell (refer Fig. S4). For convenience, the NVPF-C full-cell (NFC) with PC:DMC + FEC, EC:DMC + FEC, and EC:PC:DMC + FEC as electrolyte solvents are abbreviated as NFC-1, NFC-2, NFC-3, and NFC-4. Fig. 5 shows the charge–discharge curves as well as the long-term performance of the full-cells. After 90 cycles at 50 mA g^{-1}, NFC-1 maintained maximum of its initial capacity (60.5%, initial charge capacity: 300 mAh g^{-1}) while NFC-2 could only retain 39% of its initial capacity (initial charge capacity: 374 mAh g^{-1}).

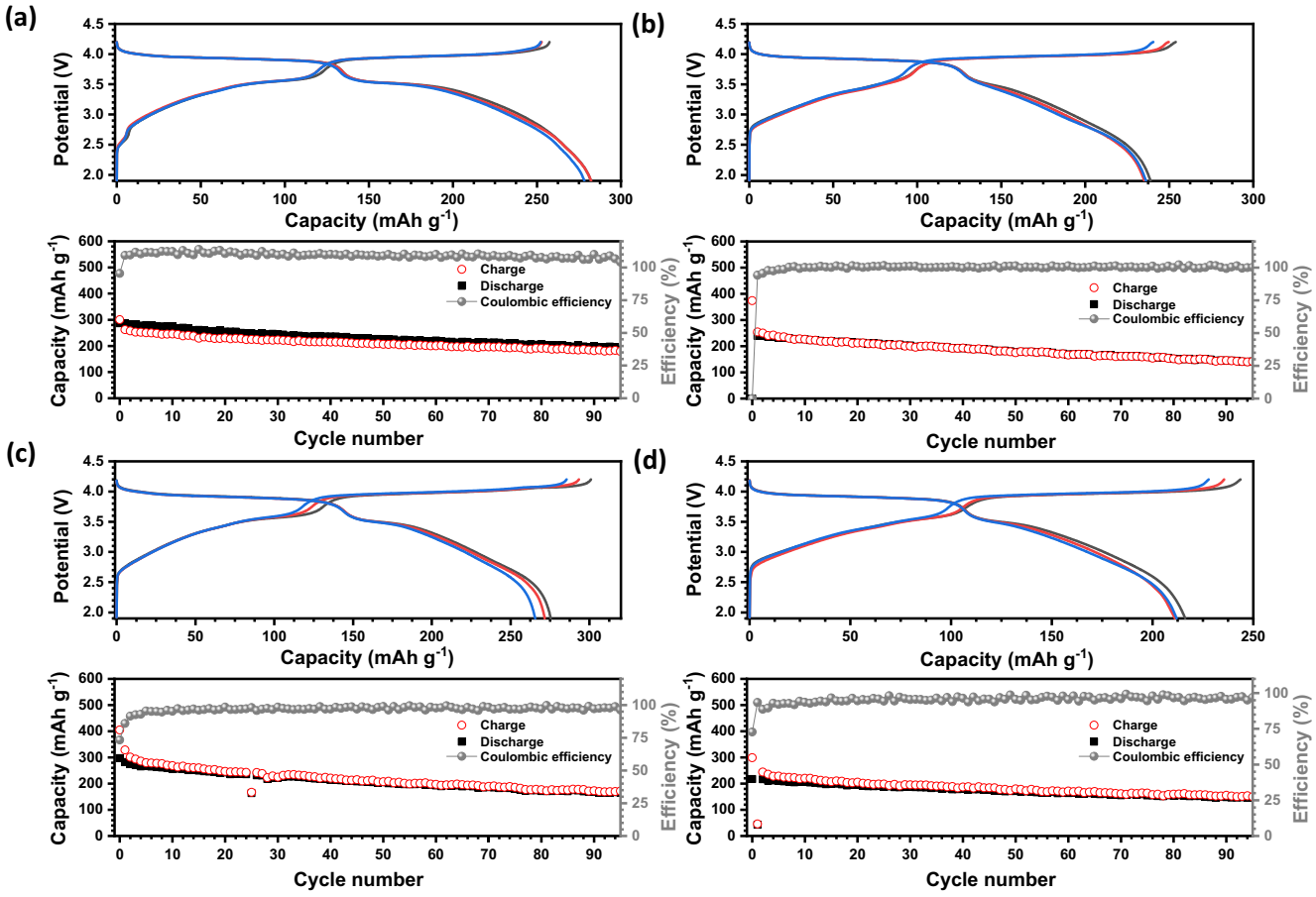

Fig. 5. Typical charge–discharge curves and the long-term cycling performance of HC/NVPF-C full-cells with 1 M $NaClO_4$ in (a) PC:DMC + FEC, (b) EC:DMC + FEC, (c) EC:PC, and (d) EC:PC:DMC + FEC electrolytes at 50 mA g^{-1} from 1.9 to 4.2 V.

The NFC-3 managed to maintain 39% of its initial capacity (initial charge capacity: 405 mAh g^{-1}), and NFC-4 managed to maintain 52% of its initial capacity (initial charge capacity: 299 mAh g^{-1}). The data proves that PC:DMC + FEC indeed is a better solvent for the half-cell and the full-cell. EC:PC has been reported as the best solvent combination for hard carbon-based cells, but failed to maintain it for this particular HC/NVPF-C full-cell. Moreover, the *in-situ* impedance could predict this outcome to a certain extent, making it an ideal tool for comparing and predicting cell performances. The rate performances of the full-cells were also evaluated (Fig. 6). The cells initially underwent two cycles at 50 mA g^{-1} to remove the irreversibility and facilitate good SEI layer formation. NFC-1 clearly shows maximum capacity retention even after cycling at 1500 mA g^{-1} with better capacity, whereas NFC-2 and NFC-3 show a maximum drop in capacity after high rate testing. Besides, NFC-3 and NFC-4 show meager capacity at 1500 mA g^{-1}, whereas NFC-1 and NFC-2 do way better. By setting the criteria as the cell that displayed maximum capacity retention after the high-rate cycling, it's seen that though NFC-2 can display higher capacity values after high-rate cycling, the capacity value at 50 mA g^{-1} is very less when compared to its value initially at 50 mA g^{-1}. But NFC-1 can retain almost all of its capacity even after cycling at such high current rates. This makes NFC-1 a better cell than others in rate performance studies due to its ability to retain the capacity even after rigorous testing at high current rates. Considering all of the above factors, clearly the electrolyte with PC:DMC + FEC as the solvent has the upper hand amongst all the electrolytes considered here in this work.

To further evaluate this superior performance of NHC-1, a temperature-dependent study was conducted using the cell that was earlier subjected to the rate study (Fig. 7). The performance was seen to be low at 0 °C, which may be accounted for by the increase in impedance due to the reduction in ionic mobility. Contrary to this, at 40 °C, the cell displayed its best performance, and at 50 °C, the capacity started fading drastically. To observe this performance, NFC-1 was subjected to long-term cycling at 50 °C, which is shown in Fig. S5. NHC-1 exhibited decent temperature performance at moderately low and high temperatures, but the poor performance at low temperatures and rapid capacity decay at high capacity. The rapid loss in capacity at high temperatures results from the decomposition of the electrolyte and the cell components.

4. Conclusion

SIB research is more focused on developing high-performance anodes and cathodes. In contrast, minimal effort is being put into the study of electrolytes, which is a crucial component to enhance cell performance. The electrolyte combination can drastically affect the cell performance, which is a distinct fact seen in this study. Carbonate-based electrolyte systems have been assiduously tested for LIB. Testing carbonate-based electrolytes for SIBs are not rehashing the ideas implemented in LIB, but a chance to revamp these. The performance of NVFP-C in half-cell assembly revealed that NHC-1 exhibited better performance out of NHC-2,3, and 4, whereas the long-term and the rate performance of the HC/

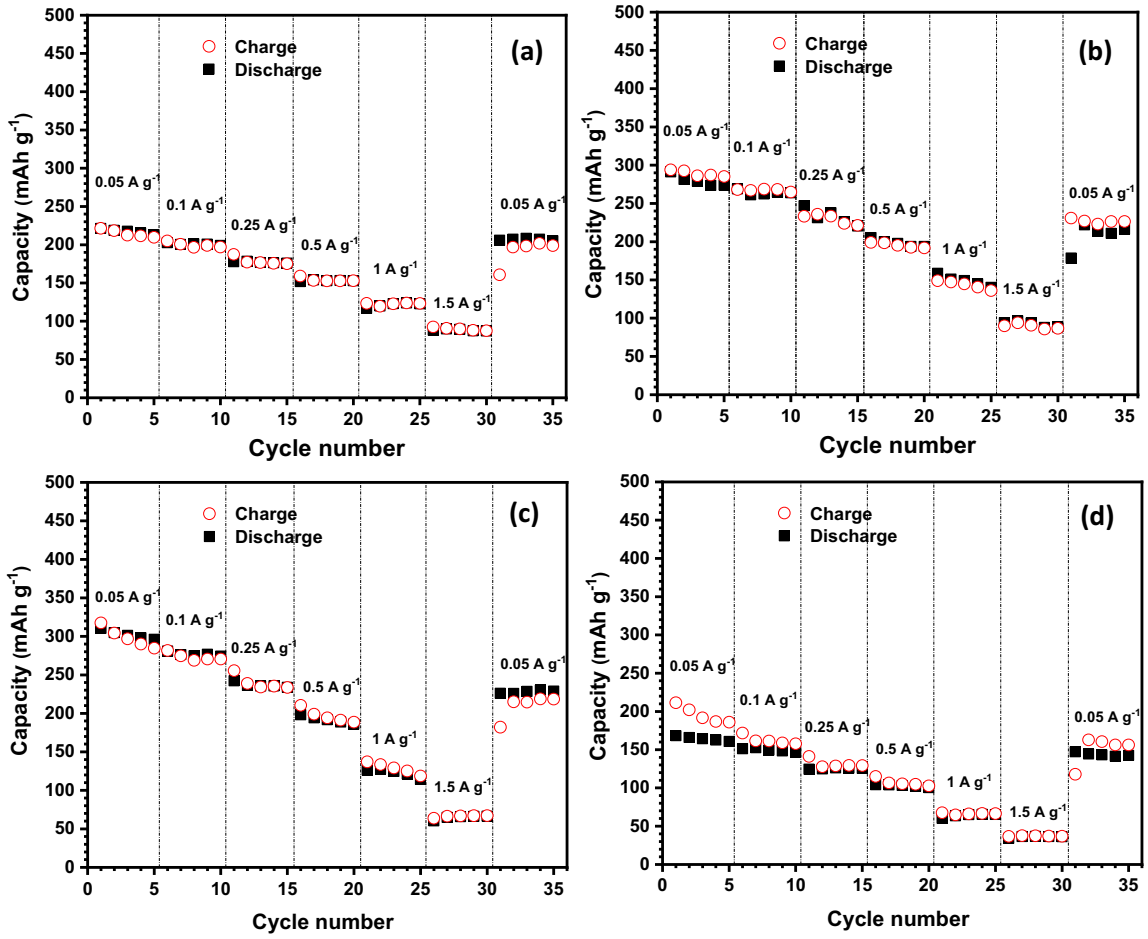

Fig. 6. Rate performances for HC/NVPF-C full-cells with 1 M $NaClO_4$ in (a) PC:DMC + FEC, (b) EC:DMC + FEC, (c) EC:PC, and (d) EC:PC:DMC + FEC electrolytes at 50, 100, 250, 500, 1000, 1500, 50 mA g^{-1} from 1.9 to 4.2 V.

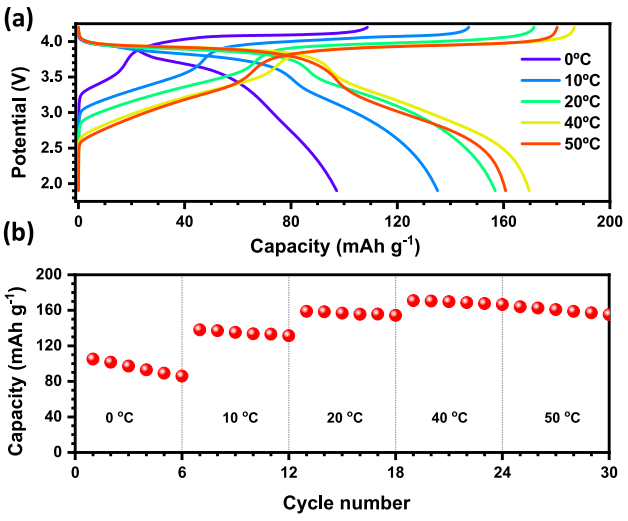

Fig. 7. Temperature study of HC/NVPF-C full-cell with PC:DMC + FEC as its solvent at current density 50 mA g^{-1} (a) Charge-discharge curves at various temperatures: 0 °C, 10 °C, 20 °C, 40 °C, and 50 °C, (b) Plot of discharge capacity *vs.* cycle number at 0 °C, 10 °C, 20 °C, 40 °C, and 50 °C for 6 cycles at each temperature.

NVPF-C full-cells also showed that NFC-1 is better than NFC-2,3, and 4. The above studies confirm that 1 M $NaClO_4$ in PC:DMC + FEC is indeed the best electrolyte among the various combination of carbonate-based electrolytes evaluated in this work. A temperature study was also performed in this work to assess this superior nature of this electrolyte system. In-situ impedance can be adopted as an excellent tool to predict the electrolyte's performance, which is a very novel approach and, to the best of our knowledge, has not been utilized for such studies. The presence of the additive and the electrode materials might have played vital roles in obtaining such a result [11–14]. The best electrolyte choice has been determined through electrochemical techniques. Additional work has to be done with the physical properties of the electrolyte, the composition of the SEI film, etc. We hypothesize that a robust and highly conductive passivation layer catapults the solvent combination PC:DMC + FEC into the best choice, and this is hinted in the impedance study. Additional contributing factors have to be looked into and would make ground for an exciting study. The electrode–electrolyte chemistry should also be explored in-depth. Unlike LIB technology, research is still going on to find a universal electrolyte for SIB technology. More work has to be done at this angle to achieve this.

CRediT authorship contribution statement

Krishnan Subramanyan: Conceptualization, Methodology, Data curation, Investigation, Writing - original draft. **Yun-Sung Lee:** Writing - review & editing, Investigation, Resources. **Vanchiappan Aravindan:** Conceptualization, Writing - review & editing, Supervision, Project administration.

Declaration of Competing Interest

The authors declare that they have no known competing financial interests or personal relationships that could have appeared to influence the work reported in this paper.

Acknowledgments

KS thanks the Department of Science & Technology (DST), Govt. of India for financial support through the INSPIRE fellowship (IF180157). YSL acknowledges the financial support from the National Research Foundation of Korea (NRF) grant funded by the Korea government (Ministry of Science, ICT & Future Planning) (No. 2019R1A4A2001527). VA acknowledges financial support from the Science & Engineering Research Board (SERB), a statutory body of the DST, Govt. of India, through the Ramanujan Fellowship (SB/S2/RJN-088/2016).

Appendix A. Supplementary material

Supplementary data to this article can be found online at https://doi.org/10.1016/j.jcis.2020.08.043.

References

[1] B. Dunn, H. Kamath, J.-M. Tarascon, Electrical energy storage for the grid: a battery of choices, Science 334 (6058) (2011) 928–935, https://doi.org/10.1126/science:1212741.
[2] J.-M. Tarascon, M. Armand, Issues and challenges facing rechargeable lithium batteries, Nature 414 (2001) 359–367, https://doi.org/10.1038/35104644.
[3] S. Natarajan, V. Aravindan, Burgeoning prospects of spent lithium-ion batteries in multifarious applications, Adv. Energy Mater. 8 (2018) 1802303, https://doi.org/10.1002/aenm.201802303.
[4] V. Aravindan, S. Jayaraman, F. Tedjar, S. Madhavi, From electrodes to electrodes: building high-performance li-ion capacitors and batteries from spent lithium-ion battery carbonaceous materials, ChemElectroChem 6 (2019) 1407–1412, https://doi.org/10.1002/celc.201801699.
[5] K. Subramanyan, V. Aravindan, Stibium: a promising electrode toward building high-performance na-ion full-cells, Chem. 5 (2019) 3096–3126, https://doi.org/10.1016/j.chempr.2019.08.007.
[6] K. Liu, Y. Liu, D. Lin, A. Pei, Y. Cui, Materials for lithium-ion battery safety, Sci. Adv. 4 (2018) eaas9820, https://doi.org/10.1126/sciadv.aas9820.
[7] P.G. Balakrishnan, R. Ramesh, T.P. Kumar, Safety mechanisms in lithium-ion batteries, 155 (2006) 401–414. https://doi.org/10.1016/j.jpowsour.2005.12.002
[8] C. Vaalma, D. Buchholz, M. Weil, S. Passerini, A cost and resource analysis of sodium-ion batteries, Nat. Rev. Mater. 3 (2018) 18013, https://doi.org/10.1038/natrevmats.2018.13.
[9] V. Aravindan, M. Ulaganathan, S. Madhavi, Research progress in Na-ion capacitors, J. Mater. Chem. A. 4 (2016) 7538–7548, https://doi.org/10.1039/C6TA02478E.
[10] S. Natarajan, K. Subramanyan, V. Aravindan, Focus on spinel Li4Ti5O12 as insertion type anode for high-performance Na-ion batteries, Small 15 (2019) 1904484, https://doi.org/10.1002/smll.201904484.
[11] C. Bommier, X. Ji, Electrolytes, SEI formation, and binders: a review of nonelectrode factors for sodium-ion battery anodes, Small 14 (2018) 1–20, https://doi.org/10.1002/smll.201703576.
[12] A. Ponrouch, R. Dedryvère, D. Monti, A.E. Demet, J.M. Ateba Mba, L. Croguennec, C. Masquelier, P. Johansson, M.R. Palacín, Towards high energy density sodium ion batteries through electrolyte optimization, Energy Environ. Sci. 6 (2013) 2361–2369, https://doi.org/10.1039/C3EE41379A.
[13] A. Ponrouch, E. Marchante, M. Courty, J.-M. Tarascon, M.R. Palacín, In search of an optimized electrolyte for Na-ion batteries, Energy Environ. Sci. 5 (2012) 8572–8583, https://doi.org/10.1039/C2EE22258B.
[14] A. Bhide, J. Hofmann, A. Katharina Dürr, J. Janek, P. Adelhelm, Electrochemical stability of non-aqueous electrolytes for sodium-ion batteries and their compatibility with Na0.7CoO2, Phys. Chem. Chem. Phys. 16 (2014) 1987–1998, https://doi.org/10.1039/C3CP53077A.
[15] D. Monti, A. Ponrouch, M.R. Palacín, P. Johansson, Towards safer sodium-ion batteries via organic solvent/ionic liquid based hybrid electrolytes, J. Power Sources. 324 (2016) 712–721, https://doi.org/10.1016/j.jpowsour.2016.06.003.
[16] C. Vidal-Abarca, P. Lavela, J.L. Tirado, A.V. Chadwick, M. Alfredsson, E. Kelder, Improving the cyclability of sodium-ion cathodes by selection of electrolyte solvent, J. Power Sources 197 (2012) 314–318, https://doi.org/10.1016/j.jpowsour.2011.09.008.
[17] G.G. Eshetu, G.A. Elia, M. Armand, M. Forsyth, S. Komaba, T. Rojo, S. Passerini, Electrolytes and interphases in sodium-based rechargeable batteries: recent advances and perspectives, Adv. Energy Mater. 2000093 (2020), https://doi.org/10.1002/aenm.202000093.
[18] A. Ponrouch, D. Monti, A. Boschin, B. Steen, P. Johansson, M.R. Palacín, Non-aqueous electrolytes for sodium-ion batteries, J. Mater. Chem. A. 3 (2015) 22–42, https://doi.org/10.1039/c4ta04428b.
[19] H. Che, S. Chen, Y. Xie, H. Wang, K. Amine, X.-Z. Liao, Z.-F. Ma, Electrolyte design strategies and research progress for room-temperature sodium-ion batteries, Energy Environ. Sci. 10 (2017) 1075–1101, https://doi.org/10.1039/C7EE00524E.
[20] K. Vignarooban, R. Kushagra, A. Elango, P. Badami, B.-E. Mellander, X. Xu, T.G. Tucker, C. Nam, A.M. Kannan, Current trends and future challenges of electrolytes for sodium-ion batteries, Int. J. Hydrogen Energy. 41 (2016) 2829–2846, https://doi.org/10.1016/j.ijhydene.2015.12.090.
[21] Z. Zuo, Y. Li, Emerging electrochemical energy applications of graphdiyne, Joule. 3 (2019) 899–903, https://doi.org/10.1016/j.joule.2019.01.016.
[22] L. Li, Z. Zuo, F. Wang, J. Gao, A. Cao, F. He, Y. Li, In situ coating graphdiyne for high-energy-density and stable organic cathodes e2000140, Adv. Mater. 32 (2020), https://doi.org/10.1002/adma.202000140.
[23] Y. Du, W. Zhou, J. Gao, X. Pan, Y. Li, Fundament and application of graphdiyne in electrochemical energy, Acc. Chem. Res. 53 (2020) 459–469, https://doi.org/10.1021/acs.accounts.9b00558.
[24] A. Ponrouch, A.R. Goñi, M.R. Palacín, High capacity hard carbon anodes for sodium ion batteries in additive free electrolyte, Electrochem. Commun. 27 (2013) 85–88, https://doi.org/10.1016/j.elecom.2012.10.038.
[25] W. Song, X. Ji, J. Chen, Z. Wu, Y. Zhu, K. Ye, H. Hou, M. Jing, C.E. Banks, Mechanistic investigation of ion migration in Na3V2(PO4)2F3 hybrid-ion batteries, Phys. Chem. Chem. Phys. 17 (2015) 159–165, https://doi.org/10.1039/c4cp04649h.
[26] W. Song, S. Liu, A sodium vanadium three-fluorophosphate cathode for rechargeable batteries synthesized by carbothermal reduction, Solid State Sci. 15 (2013) 1–6, https://doi.org/10.1016/j.solidstatesciences.2012.09.012.
[27] P.R. Kumar, Y.H. Jung, D.K. Kim, Influence of carbon polymorphism towards improved sodium storage properties of Na3V2O2x(PO4)2F3-2x, J. Solid State Electrochem. 21 (2017) 223–232, https://doi.org/10.1007/s10008-016-3365-6.
[28] A. Fujimoto, Y. Yamada, M. Koinuma, S. Sato, Origins of sp3C peaks in C1s X-ray photoelectron spectra of carbon materials, Anal. Chem. 88 (2016) 6110–6114, https://doi.org/10.1021/acs.analchem.6b01327.
[29] H. Jin, J. Dong, E. Uchaker, Q. Zhang, X. Zhou, S. Hou, J. Li, G. Cao, Three dimensional architecture of carbon wrapped multilayer Na3V2O2(PO4)2F nanocubes embedded in graphene for improved sodium ion batteries, J. Mater. Chem. A. 3 (2015) 17563–17568, https://doi.org/10.1039/C5TA03164H.
[30] X. Lin, Z. Shen, T. Han, J. Liu, J. Huang, P. Zhou, H. Zhang, J. Liu, J. Li, J. Li, Hydrogel assisted synthesis of Li3V2(PO4)3 composite as high energy density and low-temperature stable secondary battery cathode, J. Alloys Compd. 739 (2018) 837–847, https://doi.org/10.1016/j.jallcom.2017.12.348.
[31] A. Criado, P. Lavela, G.F. Ortiz, J.L. Tirado, S. Gzouli, Z. Edfouf, C. Pérez-Vicente, CTAB-assisted synthesis of C@Na3V2(PO4)2F3 with optimized morphology for application as cathode material for Na-ion batteries, Front. Phys. 7 (2019) 207, https://doi.org/10.3389/fphy.2019.00207.
[32] S.-M. Oh, S.-T. Myung, C.S. Yoon, J. Lu, J. Hassoun, B. Scrosati, K. Amine, Y.-K. Sun, Advanced Na[Ni0.25Fe0.5Mn0.25]O2/C–Fe3O4 sodium-ion batteries using EMS electrolyte for energy storage, Nano Lett. 14 (2014) 1620–1626, https://doi.org/10.1021/nl500077v.
[33] G. Yan, D. Alves-dalla-corte, W. Yin, N. Madern, Assessment of the electrochemical stability of carbonate-based electrolytes in na-ion batteries assessment of the electrochemical stability of carbonate-based electrolytes in Na-ion batteries, 2018, https://doi.org/10.1149/2.0311807jes
[34] A.V. Cresce, S.M. Russell, O. Borodin, J.A. Allen, M.A. Schroeder, M. Dai, J. Peng, M.P. Gobet, S.G. Greenbaum, R.E. Rogers, K. Xu, Solvation behavior of carbonate-based electrolytes in sodium ion batteries, Phys. Chem. Chem. Phys. 19 (2017) 574–586, https://doi.org/10.1039/C6CP07215A.